Nucleic Acids Research, 2025, **53**, gkae1157
https://doi.org/10.1093/nar/gkae1157
Advance access publication date: 3 December 2024
Structural Biology

Enzymatic bypass of G-quadruplex structures containing oxidative lesions

Peter Podbevšek [1,*] **and Janez Plavec** [1,2,3,*]

[1]Slovenian NMR Centre, National Institute of Chemistry, Hajdrihova 19, 1000 Ljubljana, Slovenia
[2]EN-FIST Center of Excellence, Trg Osvobodilne fronte 13, 1000 Ljubljana, Slovenia
[3]Faculty of Chemistry and Chemical Technology, University of Ljubljana, Večna pot 113, 1000 Ljubljana, Slovenia

[*]To whom correspondence should be addressed. Tel: +386 1 4760 240; Fax: +386 1 4760 300; Email: peter.podbevsek@ki.si
Correspondence may also be addressed to Janez Plavec. Email: janez.plavec@ki.si.

Abstract

The function of many DNA processing enzymes involves sliding along the double helix or individual DNA strands. Stable secondary structures in the form of G-quadruplexes are difficult for such enzymes to bypass. We used a polymerase stop assay to determine which structural features of the human telomeric and the BCL2 promoter G-quadruplexes can stall progression of the Klenow fragment. Primer extension profiles revealed that G-quartets are effective roadblocks for the Klenow fragment, while auxiliary base pairs can be easily bypassed. Furthermore, we utilized 8-oxoguanine to simulate oxidative damage in G-rich regions and determine the effects on enzyme bypass. In rare cases, oxidative lesions reduce the level of G-quadruplex bypass. In general, however, oxidative lesions reduce G-quadruplex stability and facilitate bypassing of such G-rich regions, especially if the lesion persists in unfolding intermediates. Our findings using Klenow fragment can be extrapolated to other G-quadruplex forming sequences and enzymes that utilise a clamp-like structure to slide along DNA and are involved in processes such as gene expression regulation and telomere maintenance.

Graphical abstract

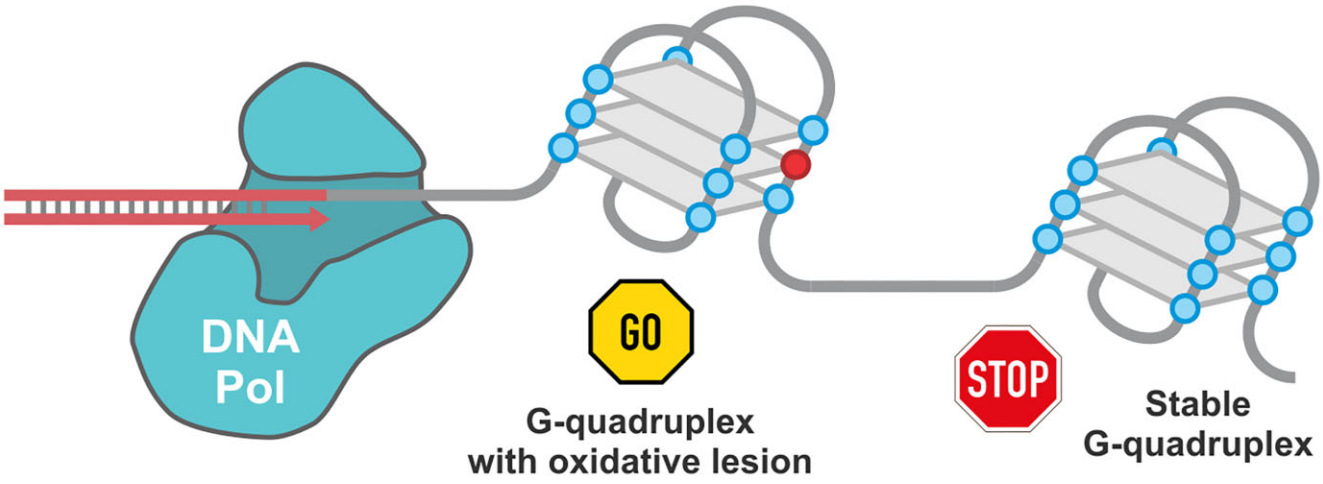

Introduction

Genomic DNA undergoes processing by a variety of enzymes. Some enzymes can directly act on double-stranded, helical DNA. Others exclusively process single strands, which necessitates (local) denaturation of the double helix beforehand. During replication of the double helix, DNA polymerase processes each DNA strand. Special proteins, helicases, assist in separating the hybridised strands in an ATP-dependent manner. However, genomic DNA can also adopt non-canonical structures, such as the four-stranded G-quadruplex (G4) (1). These can form within a single G-rich DNA strand, while the complementary C-rich strand is either single-stranded or forms the so-called I-motif structure (2). Replication catalysed by DNA polymerase can be arrested by G4 structures (3). In cells, complex machinery is required to bypass G4 structures, and failure to do so can lead to genetic instability (4,5). Re-

Received: June 7, 2024. **Revised:** October 11, 2024. **Editorial Decision:** October 31, 2024. **Accepted:** November 6, 2024

cently, several G4-specific helicases have been discovered that can assist DNA polymerases and other enzymes in bypassing G-rich regions (6). Structure-dependent stalling of DNA polymerases can be used to probe for stable G4 structures *in vitro*. G4s are notoriously polymorphic and can exhibit complex folding patterns with multiple intermediates (7,8). Analogously, their unfolding is not a simple two-state process (9,10). The degree of stalling of the polymerase generally correlates with the thermodynamic parameters of G4s, which can vary widely depending on the number of G-quartet planes, loop topology, salt or pH conditions and so on. However, thermal denaturation is fundamentally different from enzymatic unfolding. In the case of temperature-induced denaturation, all structural elements (such as G-tracts, capping structures, etc.) are available for local melting. On the other hand, enzymes often slide on the DNA double helix or single strand and approach a G4 from either the 5′- or 3′-end. A DNA polymerase will attempt to replicate the G-rich template strand in the 3′ > 5′ direction. Therefore, once an enzyme encounters a G4 structure, it must access the nucleotides involved in G4 formation in a sequential manner.

Polymerase stop assays have previously been used to study replication rates of templates adopting different types of non-canonical structures (11). Parallel and antiparallel G4s were found to be competent barriers to DNA polymerase, while hybrid G4s were easier to bypass. Similar approaches have been used to identify locations of G4 structures or to evaluate the stabilizing effect of ligand binding to G4 structures (12–16). Another study showed that although G4s can effectively stop DNA polymerase, at higher concentrations the polymerase can oligomerize and disrupt G4 structures, leading to an easier bypass of G-rich regions (17). We have previously shown that a G4 structure adopted by the vascular endothelial growth factor (VEGF) gene can be disrupted by 8-oxoG and recovered by a short ligand-conjugated G-tract (18). In a subsequent study, the efficacy of different ligands to recover damaged G4 structures was evaluated with a polymerase stop assay (19).

G-rich regions of DNA are highly susceptible to oxidative damage, which can have a significant impact on the structure and stability of G4s. A major product of G oxidation is 8-oxo-7,8-dihydroguanine (8-oxoG) and is commonly used as a biomarker for oxidative stress (20,21). We have previously studied G-rich sequences derived from the promoter region of B-cell lymphoma 2 (BCL2) and the human telomeric region (HTEL), both known for their propensity to form G4 structures. Replacing guanines with 8-oxoG is generally detrimental to the thermal stability of G4. Nevertheless, two HTEL-derived G4 structures have been characterized and shown to incorporate 8-oxoG into their G-quartets (22). Replacing a G that was originally in the *syn* conformation resulted in only minor structural adjustments. On the other hand, replacing a G originally in the *anti* conformation with an 8-oxoG resulted in a major conformational shift from hybrid-1 to hybrid-2 G4 topology. This enabled 8-oxoG to adopt its preferred *syn* conformation. The BCL2 promoter contains multiple G-tracts of different lengths. In a unique case, we observed a significant increase in the thermal stability of G4 after replacing a specific G with 8-oxoG within a BCL2-derived construct (23). While the original G is part of a G-quartet, replacement with 8-oxoG leads to a register shift in the long G-tract in conjunction with a rearrangement of the *syn* and *anti* G conformations. This repositioning displaces 8-oxoG from the G4 core into the loop region, where it base pairs with loop nucleotides to form an extensive capping structure.

Given 8-oxoG's capability to modulate the thermal stability of G4 structures, we anticipated that associated structural features are able to significantly impact the rate at which enzymes process G-rich regions containing 8-oxoG. In the current study, we investigated the ability of the Klenow fragment (KF) to unfold and replicate G-rich templates derived from BCL2 and HTEL that contain an oxidative lesion, 8-oxoG (Figure 1A). Analysis of primer extension reactions enabled us to quantify stalled products at different temporal stages of the reaction with single nucleotide resolution. Data on the progression of KF were coupled with previously determined high-resolution structures of BCL2 and HTEL G4s to reveal structural features relevant to modulation of KF bypass. We have found G-quartets to be effective barriers for replication. However, 8-oxoG can alleviate KF bypass, particularly when positioned in a G-tract closer to the 5′-end of the G-rich template. Our data corroborate the importance of 'spare tyres' in G-rich regions of promoters that allow the exclusion of oxidative lesions from G-quartets in order to maintain G4 structure and function.

Materials and methods

Sample preparation

All oligonucleotides were synthesized on a K&A Labs DNA/RNA Synthesizer H-8 using standard phosphoramidite chemistry. 6-Fluorescein phosphoramidite (6-FAM) (Glen Research) was added to the 5′- end of the primers used in the polymerase stop assay. The oligonucleotides were deprotected with AMA (1:1 mixture of aqueous ammonium hydroxide and methylamine) at 65°C for 15 min. The DNA was purified using Glen-Pak reverse-phase purification cartridges (Glen Research). Additionally, the oligonucleotides were desalted using FPLC and a HiPrep Sephadex G25 column (GE). DNA solutions were dried in a vacuum centrifuge and redissolved in 20 mM potassium phosphate buffer, pH 7, and 70 mM KCl. DNA concentrations were determined by measuring UV absorbance at 260 nm using extinction coefficients calculated with the nearest-neighbour method.

NMR spectroscopy

All NMR data were collected with Bruker 600 MHz NMR spectrometers equipped with cold probes. All samples used for NMR contained 20 mM potassium phosphate buffer, pH 7, 70 mM KCl and 5% $^{2}H_2O$. Spectra were acquired at 25°C using excitation sculpting solvent suppression. DNA concentration was 150 μM per strand.

UV melting

Melting temperatures of G-rich oligonucleotides forming G4 structures were determined using the same ionic conditions as for the template extension reactions. This included 50 mM KCl, 10 mM Tris–HCl, pH 7.9 and 10 mM $MgCl_2$. The DNA was taken from NMR samples and diluted to a target absorbance range between 0.3 and 0.5. Absorbance was measured at 295 nm and the temperature was increased from 15 to 95°C with a 0.5°C/min gradient. A sig-

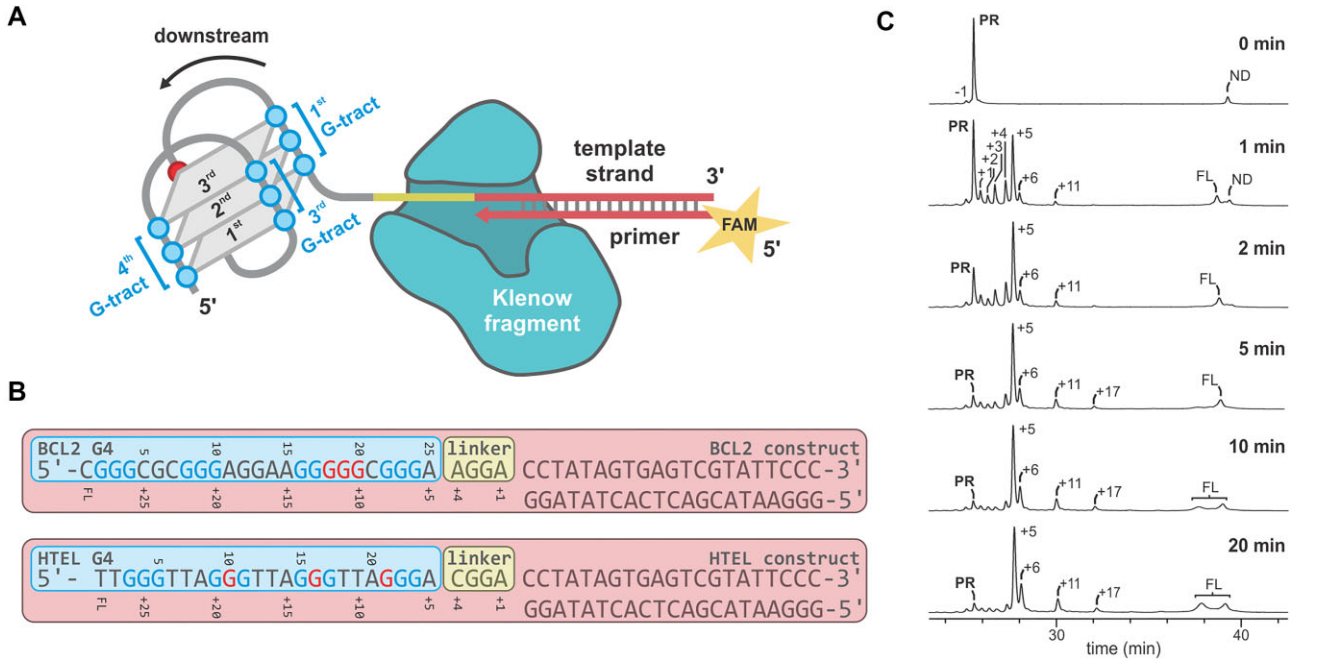

Figure 1. (**A**) Polymerase stop assay using a fluorescently (FAM) labelled primer. Stable secondary structure elements such as G4s impede the replication of the template strand. (**B**) Sequences of BCL2 and HTEL constructs comprised of G4 forming sequences, short linkers and regions with hybridised primers. Stalled products are labelled by the number of nucleotides added (+X). Positions where 8-oxoG was introduced into G-rich regions are labelled in red. (**C**) A representative set of electropherograms (using HTEL as an example) taken at different times of the primer extension reaction. The primer (PR) is extended by a different number of nucleotides (+1, +2, +3, etc., up to full length, FL).

moidal function was fitted to the data points to extract the T_m values.

Polymerase stop assay

Primer extension reactions with a total volume of 300 µl contained 1 µM template DNA, 1 µM fluorescent primer, dNTP mix (50 µM each, Jena Bioscience), 50 mM KCl, 10 mM Tris–HCl, pH 7.9, 10 mM $MgCl_2$ and 1 mM DTT. With random control constructs (RND) KCl was replaced with 50 mM LiCl. A 50 µl aliquot was taken as a negative control before 2 U of the KF (3′-5′ exo$^-$, NEB) were added to the remaining 250 µl and the reaction was incubated in a water bath at 25°C. Five subsequent aliquots were collected at 1, 2, 5, 10 and 20 min. The reaction in all aliquots was quenched immediately with 1 µl of 0.5 M EDTA, followed by thermal denaturation at 75°C for 10 min. Subsequently, 5 µl of 3 M NaOAc and 200 µl of EtOH were added and the DNA was precipitated overnight at −80°C to reduce the ionic strength of the samples. Next, all samples were centrifuged extensively. The supernatant was discarded and the pellets were air-dried. Samples corresponding to the different reaction times were redissolved in 100 µl H_2O and used as stock solutions. These solutions contained the non-fluorescent template strand and fluorescent primer extension products of different lengths.

Capillary electrophoresis

The purified DNA was diluted and denatured prior to analysis. Thermal denaturation proved detrimental to the fluorescent tag. Therefore, 60% DMSO was used as a denaturant, as increasing the ionic strength would hinder efficient electrokinetic injection. The samples for capillary electrophoresis (CE) contained 1 µl of DNA stock solution, 19 µl of H_2O and 30 µl of DMSO. The use of more DNA resulted in higher fluorescence, but DMSO was less effective in denaturing the hybridised DNA, resulting in intense broad peaks in the electropherograms.

An Agilent 7100 CE system was coupled to an Adelis Zetalif laser-induced fluorescence detector with a 488 nm laser. This enabled us to detect only the primer extension products and not the template strand. Laser power was set to 20 mW and the voltage of the photomultiplier to 570 V. Initially, a coated Agilent µSIL- DNA capillary was used. However, a non-coated Polymicro fused silica capillary with an internal diameter of 100 µm showed comparable performance and was used in all tests. The total length of the capillary was 52 cm, with an effective length (to the detector) of 31 cm. CE was performed with inverse polarity and a voltage of −25 kV. The DNA was injected electrokinetically for 10 s and −10 kV. A mixture of 200 mM BisTris and 200 mM boric acid was used as electrolyte solution. The polymeric solution contained 15% PEG 35000 with 20% (v:v) acetonitrile, 160 mM BisTris and 160 mM boric acid. The capillary was filled with a fresh polymer solution under high pressure (5 min, 5 bar) before each analysis.

Peaks in electropherograms could be unambiguously assigned, starting from the non-extended primer (PR). Low intensity, but well-resolved, peaks were present for all extended primers and could be easily counted with a single nucleotide resolution. All peaks with a total area >1% were integrated. Peak area ratios were used to plot stacked area charts as a function of reaction time. BCL2 and HTEL were selected as representative cases, and all experiments were conducted in triplicates. Variations are minimal (Supplementary data) and average values are reported.

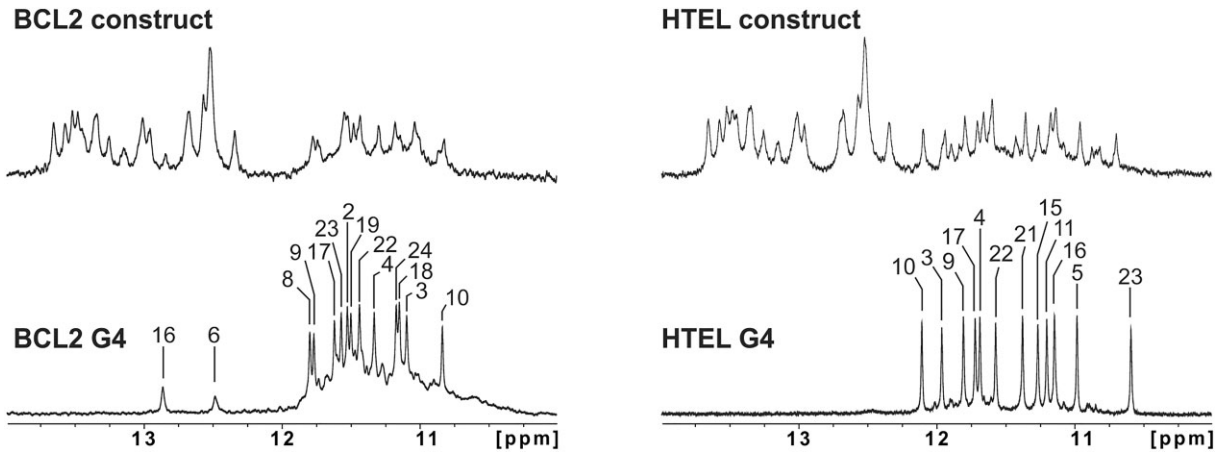

Figure 2. Imino regions of 1D ^{1}H NMR spectra of 25-nt BCL2 G4 and 24-nt HTEL G4 with assignment (lower) compared to 50-nt BCL2 and 49-nt HTEL constructs with 21-nt primers (upper). Spectra were acquired at 600 MHz with 150 μM DNA (per strand), 20 mM KPi buffer (pH 7) and 70 mM KCl.

Results

G4 structure is not affected by hybridisation with primers

We have selected two G-rich sequences with known high-resolution structures as model systems. 25-nt and 24-nt sequences derived from the human BCL2 promoter and HTEL, respectively, were extended at the 3′-end by a short 4-nt linker and a 21-nt primer binding region to serve as templates for primer extension (Figure 1B). BCL2 and HTEL G-rich sequences, along with their analogues containing oxidative lesions, were tested with NMR spectroscopy at ionic conditions later used for primer extension reactions. The ^{1}H NMR resonance patterns were identical to spectra of previously published high-resolution structures, which indicates that the G4 structures are not affected (Supplementary Figure S1) (22–24). Furthermore, since the extension of the original sequences could interfere with G4 formation, we tested the BCL2 and HTEL constructs comprised of template strands and fully complementary 21-nt primers. 1D ^{1}H NMR spectra of BCL2 and HTEL constructs contain resonances in the range of 10.8–12.1 ppm belonging to Hoogsteen hydrogen bonded guanines that constitute the G4 structures (Figure 2). These resonances exhibit minor chemical shift changes and broadening compared to resonances of BCL2 and HTEL G4-forming sequences. Importantly, the chemical shift patterns are in agreement, which indicates that the original G4 structures are retained in the larger constructs despite extended sequence and bound primer. NMR spectra of BCL2 and HTEL constructs also contain a number of resonances in the range of 12.1–13.6 ppm corresponding to Watson–Crick hydrogen bonded nucleotides, suggesting that the primers are fully hybridised to both template strands.

BCL2 and HTEL constructs, along with their analogues containing oxidative lesions, were mixed with KF to initiate primer extension reactions. Reaction mixtures were incubated at 25°C to ensure that G4 structures, especially those containing oxidative lesions, are not partially melted. Furthermore, a low reaction temperature slowed the progression of KF, which enabled us to monitor its progress as a function of reaction time. Aliquots of primer extension reactions were analysed by CE. Electropherograms show how efficient KF is at replicating G-rich templates and reveal some common features (Supplementary Figures S2–S9). Most aliquots contain a small fraction of the −1 fragment (Figure 1C), which is a by-product of primer synthesis and was disregarded in the subsequent quantitative analysis. Analysis of some aliquots showed a small fraction of the non-denatured template/primer hybrid (ND), which was also not considered in the subsequent analysis. All other peaks in electropherograms (between 1 and ND) were integrated and ratios of peak areas were directly used to determine molar ratios of reaction products. In case of complete blocking of KF, only the non-extended primer (PR) would be detected in the reaction mixture. On the other hand, efficient bypass of KF would yield solely full-length (FL) products. The presence of secondary structures hindering KF bypass would lead to stalled products (+1, +2, +3, etc.) with lengths that correlate with positions of secondary structure elements. Analysis of sets of electropherograms revealed that primer extension proceeds rapidly in the first few minutes of the reaction. With all studied constructs, the non-structured 4-nt linker was easily replicated by KF. In the first 10 min of reactions, a build-up of stalled products with increasing length was detected. In the following 10 min, only minor changes in molar ratios of stalled products could be observed. Therefore, we consider the primer extension to be complete after 20 min of reaction time. All molar ratios discussed hereafter are provided as of the 20 min mark, unless specified otherwise. A control construct (RND) comprised of a random non-G-rich 24-nt template sequence, d(ATTGACAGTGTTGCTCGTCCAGAC), extended by the 4-nt linker and the 21-nt primer binding region was tested to ensure KF is capable of complete bypass. Furthermore, Li^{+} was used as the counterion in these control reactions. Primer extension reactions with RND resulted in 95% FL (Supplementary Figures S10 and S11). Next, we individually replaced two guanine positions in RND with 8-oxoG. The polymerase stop assay indicated a slight degree of stalling at the 8-oxoG lesion, as well as at the adjacent upstream and downstream sites (Supplementary Figures S10, S12 and S13). The two constructs, RNDoxoG10 and RNDoxoG17, produced in total 15 and 14% of stalled products at and adjacent to the lesion, respectively. Consequently, the levels of FL products dropped to 75 and 78%, respectively.

Oxidative lesions within loop regions exert minimal impact on enzyme bypass

BCL2 adopts a basket-type G4 topology with three G-quartet planes flanked by a GCAA pseudo-quartet (Figure 3A) (23). The BCL2 G4 structure exhibits a melting temperature of 64°C (Supplementary Figure S14). When the primer is extended, the G4 structure on the template strand is approached by KF at the 3′-end. In the 3D structure of the human BCL2 G4, A25 is hydrogen-bonded to G16 and A11, and is the first nucleotide that is not fully accessible for replication. Stalling of KF upstream of A25 would lead to accumulation of the +4 stalled product. However, analysis of the electropherograms showed that A25 is relatively easy to replicate with only 8% of the +4 stalled product (Figure 3A). On the other hand, G24, the next nucleotide in the 3′ > 5′ direction, which is involved in the first G-quartet, cannot be replicated efficiently. The major stalling site in BCL2 is +5, which represents 44% of stalled products. Interestingly, 8% of the +6 stalled product was also detected, suggesting that not only replication of the first G, but also of the second G in the G4 core (to a much lesser extent) is rate-limiting in a polymerase reaction. Analysis of BCL2 reactions also revealed small fractions of +9 and +10 stalled products upstream of the next G-tract with 6 and 4%, respectively. Only 12% of the FL product were detected indicating that the BCL2 G4 is difficult for KF to bypass.

The introduction of 8-oxoG to position 18, into the centre of the long G-tract of BCL2 (G16-G20), disrupts G4 formation (23). BCL2oxoG18 was used as a control with no stable secondary structure formed in its G-rich region. Primer extension results reflect this with a significantly higher fraction of the FL product (37%) (Figure 3B). Some +5 (14%) stalled product was observed preceding the first G-tract. An equal fraction of the +13 (14%) stalled product was also observed, which includes a single nucleotide downstream of the oxidized site (8-oxoG18).

Replacing G19 with 8-oxoG induces notable changes in the folding of the BCL2 G4 region. The BCL2oxoG19 G4 features a basket-type topology with three G-quartet planes (Figure 3C) (23). It is noteworthy that the BCL2oxoG19 G4 lacks the GCAA pseudo-quartet. This is due to the repositioning of the long G-tract, where 8-oxoG19 is not involved in G-quartet formation. The register shift is accompanied by reversal of *syn*- and *anti*-conformations of equivalent Gs compared to non-oxidized BCL2 G4. This enables 8-oxoG19 to hydrogen bond with its Watson–Crick and Hogsteen sides to C21 and G6, respectively (Figure 3C). Surprisingly, the resulting base triad increases the thermal stability of the G4 structure to 74°C, which is a 10°C difference compared to the BCL2 G4 (Supplementary Figure S14). Primer extension reactions of BCL2oxoG19 show the expected stalling sites, +5 (42%), +6 (9%), involving the first G-tract (Figure 3C). Interestingly, a large fraction of the +4 stalled product (26%) indicates that A25, which is not involved in any secondary structure elements, cannot be effectively replicated. This is likely due to steric constraints of the KF active site (vide infra). Reactions with BCL2oxoG19 also revealed small fractions of +10 (3%) and +11 (4%) stalled products, which are upstream of the base triad and the second G-tract, respectively.

Our previous studies have shown that replacing G20 in BCL2 G4 with 8-oxoG has little effect on NMR spectral properties and only a small decrease in thermal stability to a T_m value of 61°C (Supplementary Figure S14), which is to be expected since G20 is located in the edge-type loop and does not base pair (23). The topology of BCL2oxoG20 G4 is identical to BCL2 G4, which is reflected in a similar primer extension profile (Figure 3D). The major stalling site in BCL2oxoG20 is +5 with a 50% fraction of total products. A notable fraction of the +9 stalled product (8%) was detected, suggesting that the oxidative lesion causes some stalling. In contrast to BCL2, the level of FL was below the detection limit, indicating that BCL2oxoG20 cannot be replicated with KF under the conditions used here.

Stability of the G4 core is controlled by the position of the lesion

G4 structures originating from the HTEL were previously shown to be affected by oxidative lesions (22). The non-oxidized HTEL G4 adopts a hybrid-1 type fold, which melts at 67°C (Figure 4A and Supplementary Figure S14) (24). The 3′-side of the G4 is flanked by a reversed Watson–Crick T13·A24 base pair. However, this does not appear to be an issue for KF as primer extension reactions show that the fraction of the +4 stalled product is very low (4%) (Figure 4A). The major stalling site in primer extension reactions with HTEL is +5 (44%), upstream of the first G-quartet. However, a substantial fraction of G23 can be replicated before KF stalls at position +6 (13%). The next significant stalling site is +11 (7%), upstream of the second G-tract. Overall, HTEL can effectively stall KF bypass with only 15% FL product.

Our previous structural studies have shown that disruption of the central G-quartet of HTEL G4 with an 8-oxoG has a pronounced destabilizing effect (22). The hybrid-2 type structure of HTELoxoG10 G4 exhibits a T_m of 42°C (Figure 4B and Supplementary Figure S14). The primer extension profile of HTELoxoG10 shows that its G4 structure is ineffective at stalling KF with 65% of FL product (Figure 4B). The only significant stalling sites are +5 (7%) and +11 (6%), upstream of the first and second G-tracts, respectively. No stalled products, which would correlate with base triads at either end of the G4 core could be detected.

HTELoxoG16 was used as a control as it exhibits poor NMR spectral properties, indicating no stable G4 structure is formed in its G-rich region (22). Nevertheless, HTELoxoG16 is not completely unstructured as few imino resonances were observed NMR spectra and some Hoogsteen and Watson–Crick base pairs are clearly formed (Supplementary Figure S1). The primer extension profile was very diverse with +14 as the major stalling site (Figure 4C), which is the nucleotide downstream of the oxidized site (8-oxoG16). Expectedly, a high fraction (30%) of FL product was observed.

Introducing 8-oxoG at position 21 yields an identical hybrid-1 type topology as the non-oxidized HTEL G4 (Figure 4D) (22). However, the thermal stability is reduced to a T_m of 52°C (Supplementary Figure S14). Primer extension reactions with HTELoxoG21 show a relatively low fraction of the +5 stalled product (15%) (Figure 4D). G23 and G22 of the first G-tract as well as 8-oxoG21 cause negligible stalling. However, KF stalls upstream of A20 and produces 9% of the +8 stalled product. We believe that this is due to the T1·A20 Watson–Crick base pair, which hinders bypass of KF. The next significant stalling site is +11 (12%), upstream of the second G-tract and finally +17 (5%) upstream of the third G-tract. The facilitated bypass of the first G-tract likely contributes to a relatively high fraction of the FL product (27%).

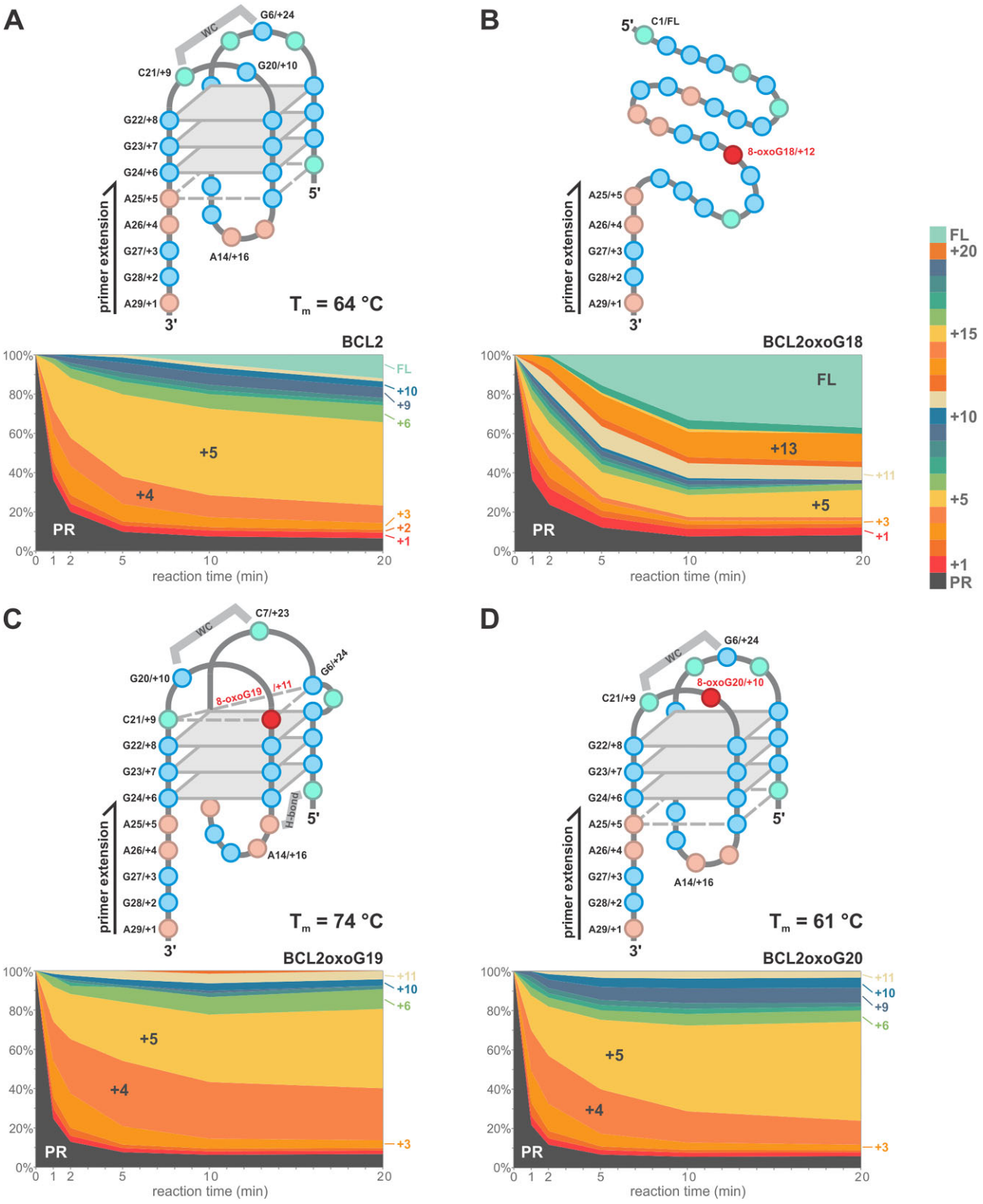

Figure 3. Topologies of structures (upper panel) and corresponding polymerase stop assay results (lower panel) for BCL2 (**A**), BCL2oxoG18 (**B**), BCL2oxoG19 (**C**) and BCL2oxoG20 (**D**). The naming convention consists of the standard nucleotide position in the 5′ > 3′ direction, followed by the length of stalled product in the 3′ > 5′ direction. G-quartets are depicted as grey planes, while base triads and pseudo-quartets are connected with a dashed line. Watson–Crick base pairs are linked with a thick line. Area charts show relative fractions of PR, individual stalled products and FL as a function of reaction time. The colour code for different stalled products is on the right. T_m values are given next to corresponding G4 topologies.

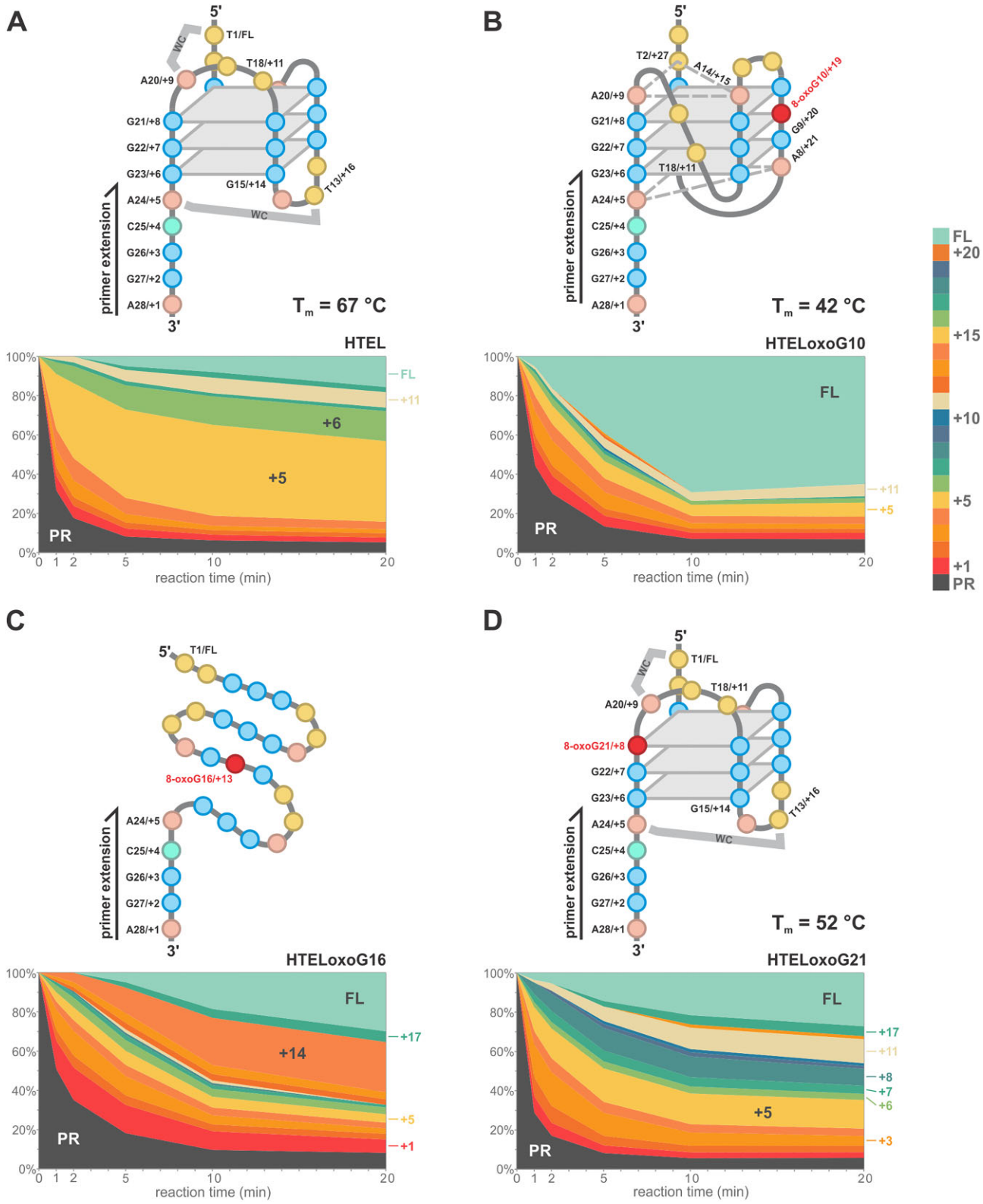

Figure 4. Topologies of structures (upper panel) and corresponding polymerase stop assay results (lower panel) for HTEL (**A**), HTELoxoG10 (**B**), HTELoxoG16 (**C**) and HTELoxoG21 (**D**). G-quartets are depicted as grey planes, while base triads are connected with a dashed line. Watson–Crick base pairs are linked with a thick line. Area charts show relative fractions of PR, individual stalled products and FL as a function of reaction time. The colour code for different stalled products is on the right. T_m values are given next to corresponding G4 topologies.

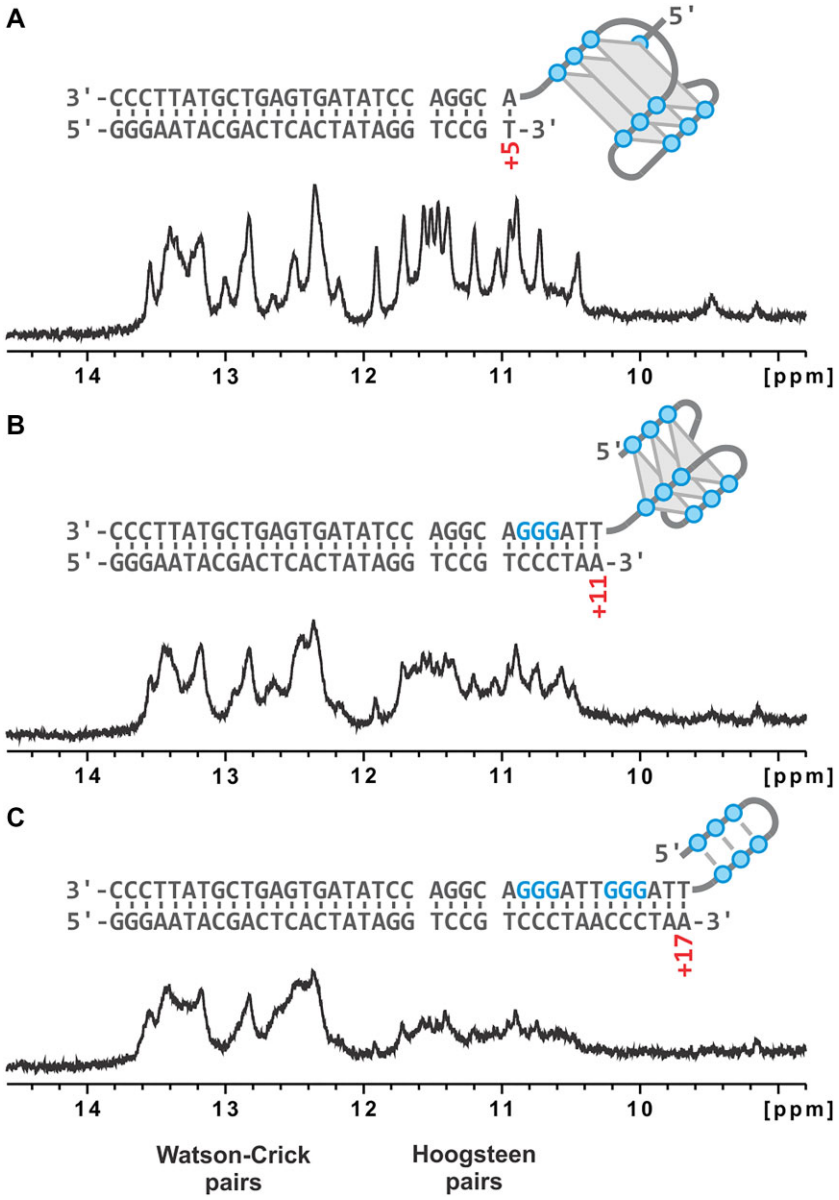

Figure 5. Imino regions of 1D ^{1}H NMR spectra of (**A**) +5, (**B**) +11 and (**C**) +17 constructs simulating stalling of KF due to unfolding intermediates progressively extended primers form Watson–Crick base pairs with the HTEL template strand. Guanines of the 5′ overhangs of template strands are able to self-associate in Hoogsteen base pairs to form (A) the G4 structure, (B) triplex structures or (C) hairpins. Spectra were acquired at 5°C on a 600 MHz with 50 μM DNA (per strand), 20 mM KPi buffer (pH 7) and 70 mM KCl.

Primer extension of a G4 forming sequence can produce unfolding intermediates

As KF progresses through the G-rich region of the template it reduces the number of available G-tracts, which can self-associate by G·G base pairing. We prepared three synthetic extended primers with lengths of 26, 32 and 38 nt, which were mixed with equimolar amounts of the 49-nt template strand. These primers correspond to stalled products reaching the first (+5), second (+11) and third (+17) G-tract of HTEL (Figure 5). The +5 construct should allow for the formation of a G-quadruplex, while the +11 and +17 constructs allow for the formation of triplexes and hairpins, respectively. Our NMR analysis confirms this by showing that all constructs exhibit Watson–Crick hydrogen bonded nucleotides (12–14 ppm) corresponding to the overlapped region between the two strands. Additionally, all constructs also exhibit Hoogsteen hydrogen bonded nucleotides (10–12 ppm), which correspond to the overhangs capable of adopting G-quadruplex, triplex or hairpin structures. Spectra were acquired at 5°C in order to slow down imino proton exchange. Nevertheless, +11 and +17 constructs exhibit ^{1}H resonances in the Hoogsteen range that are less intense compared to the Watson–Crick spectral region. This is expected due to guanines in triplexes and hairpins being more exposed to the solvent. Furthermore, +11 and +17 constructs exhibit heavily overlapped resonances in the Hoogsteen range, which suggests that the triplex and hairpin unfolding intermediates are structurally heterogenous.

Discussion

Different enzymes, even different DNA polymerases, are more or less capable of bypassing G-rich substrates. We have used a

specific DNA polymerase and an optimized set of conditions to determine how different topologies of non-canonical DNA structures, like G-quadruplexes, modulate the bypass rate and populations of stalled products relative to each other. The absolute degree of stalling is likely completely different in a cellular context. However, stalling positions and the effect of oxidative lesions should be valid *in vivo*. In our experimental setup, both BCL2 and HTEL G4 structures proved to be effective roadblocks as they significantly hindered KF bypass. This suggests that auxiliary proteins such as helicases are crucial for the processing of such G-rich genomic regions. Our results using KF can likely be extrapolated to other enzymes that employ a clamp-like structure to slide along the DNA. One such example are transcription activation complexes, which utilize a sliding clamp to scan for promoters (25). While the role of G4s in promoters is far from understood, their presence is generally associated with transcriptional repression as they interfere with polymerase processivity (26). A recent study found that this is also the case for the promoter of the BCL2 gene, where a stable G4 down-regulates the expression of this anti-apoptotic gene (27). Our data show that the BCL2 is difficult for KF to bypass. In addition, BCL2oxoG19 and BCL2oxoG20 were also very effective in stalling KF, suggesting that basal levels of gene expression are likely unaffected. These thermally stable G4 structures containing 8-oxoGs exhibit comparable or even higher thermal stability than non-oxidized BCL2 G4 (23). On the other hand, most oxidation events are detrimental to G4 structure and stability. Oxidation of these G positions should reduce G4 stability and facilitate bypass of the transcriptional machinery, leading to potential upregulation of BCL2 protein expression.

BCL2-derived G4s caused significant stalling of KF two nucleotides upstream of the first G-quartet, at position +4, indicating that A25 cannot be replicated efficiently. While A25 is a part of a pseudo-quartet in BCL2 and BCL2oxoG20, it is neither base paired nor stacked in BCL2oxoG19 and should be easily accessible for replication. We hypothesise that KF cannot position A25 in its active site due to steric constraints. It has been shown that KF interacts with up to 4 upstream nucleotides of the template strand (28). Due to a longer diagonal loop on the 3′ side of the BCL2oxoG19 G4 structure, compared to BCL2 and BCL2oxoG20, the interaction of upstream nucleotides with KF might be hindered. Moreover, A15 stacks efficiently with G24, which further stabilizes the diagonal loop in BCL2oxoG19. A structured loop combined with higher thermal stability of BCL2oxoG19 likely contributes to a higher fraction of the +4 stalled product compared to BCL2 and BCL2oxoG20. Other studies also observed polymerase stalling more than one nucleotide upstream of a stable G4 structure (5,12). Unlike BCL2-derived G4s discussed above, all primer extension profiles of HTEL-derived G4 structures exhibit only negligible amounts of the +4 stalled product. Propeller and shorter edge-type loops found in HTEL, HTELoxoG10 and HTELoxoG21 seem to be less sterically obtrusive and enable replication of A24 despite its base pairing with T13 or T7/A8. Furthermore, in HTEL reactions a significant fraction (13%) of G23 could be replicated before stalling, despite G23 constituting a stable G-quartet. This suggest that Gs in outer G-quartets are easier for KF to access than inner G-quartets.

Similarly to BCL2, most oxidation events in the HTEL have been shown to be detrimental to G4 structure. Nevertheless, some G positions have been found to tolerate 8-oxoG and retain a G4 structure, although their thermal stability decreases significantly (22). HTEL and HTELoxoG21 were shown to adopt an identical G4 topology, which allows 8-oxoG to be incorporated at position 21 without major disruption to the structure. However, HTEL can block KF much more effectively than HTELoxoG21. Full bypass increases moderately from 15% with HTEL to 27% with HTELoxoG21. This is largely due to the more efficient bypass of the first G-tract, which is indicated by a decrease in the fraction of the +5 product from 44% (HTEL) to 15% (HTELoxoG21). Interestingly, the total fraction of stalled products longer than +5 and shorter than FL increases from 26% with HTEL to 38% with HTELoxoG21. This means that even after replication of the first G-tract, it is not all smooth sailing for KF. With HTELoxoG21 there is significant stalling upstream of the second G-tract and to a lesser extent before the third G-tract. These observations suggest that the G-rich substrate is sequentially denatured via several unfolding intermediates. The initial G4 structure is gradually reduced to a triplex, a hairpin and finally undergoes complete unfolding/denaturation (29,30).

The initial dissociation of Gs in the first G-tract is probably rate-limiting for the polymerase reaction. This is likely followed by further dissociation of another G-tract, resulting in a transiently stable hairpin. Therefore, a higher degree of polymerase stalling is expected in the 3′ region of the template and less towards the 5′- end due to the lower stability of unfolding intermediates. In HTELoxoG21, 8-oxoG is located in the first G-tract, to be replicated. All unfolding intermediates in the form of triplexes and hairpins would therefore be lesion-free and relatively stable. On the other hand, HTELoxoG10 contains an 8-oxoG in the third G-tract of its G4 structure. This means that as the G4 progressively unfolds from the 3′-end, the oxidative lesion persists in both the triplex and the hairpin (Figure 6). Our primer extension assay supports this with an almost complete bypass of the HTELoxoG10 G4 by KF. Only a few per cent of the +5 and +11 product could be detected, corresponding to the stalling sites upstream of the first and second G-tract, respectively.

An important difference compared to other G4 systems described here is that HTELoxoG10 is comprised of either fully *syn* of fully *anti* G-tracts. This could allow easier strand slippage since no *syn*/*anti* reshuffling is required (29). Initially, KF would pull the first G-tract in the 3′ direction, reducing the number of complete G-quartets. This would likely destabilize the structure significantly and facilitate replication with KF. The same scenario could be repeated upstream of the second G-tract by pulling the strand and effectively reducing the number of guanine base triads. Facilitated strand slippage likely contributes to the very efficient KF bypass of HTELoxoG10.

Several previous studies have reported that KF has difficulties replicating 8-oxoG and stalls upstream of such lesions (31). However, our observations show that this is not the case, at least for the BCL2 and HTEL systems. Although some stalling was observed upstream of 8-oxoG sites, this did not exceed 8% of the total products (BCL2oxoG20). Furthermore, these stalling positions can also be attributed to structural features. Interestingly, both control samples (BCL2oxoG18 and HTELoxoG16), with no stable G4 structure, exhibit noticeable stalling a single nucleotide downstream of the oxidized site. This suggests that 8-oxoG can be replicated, while distortions caused by the newly formed 8-oxoG base pair are transmitted back to the polymerase ac-

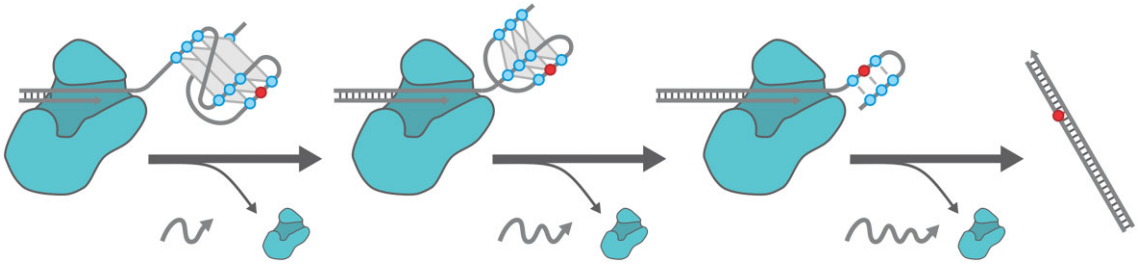

Figure 6. Proposed mechanism of KF-catalysed unfolding of a model structure of G4 (not to scale). The oxidative lesion in the third G-tract persists in all unfolding intermediates and allows KF to easily bypass the G-rich region. Small fractions of KF stall and dissociate upstream of the G4, triplex and hairpin unfolding intermediates producing progressively longer, but not full length, DNA strands.

tive site. We also observed stalling on the non-G-rich template (Supplementary Figure S10). With RNDoxoG10 KF primarily stalled upstream of the 8-oxoG site. On the other hand, RNDoxoG17 caused stalling at the 8-oxoG lesion, as well as at the adjacent upstream and downstream sites. This suggests a degree of sequence specificity affecting the level and position of stalling. However, in both cases, the total stalling at and near the lesion remained below 15%. Similar behaviour was not observed in stable G4s, where stalling of KF is the result of secondary structure elements.

As the primer extension reactions progress with time there is an accumulation of stalled products and the reactions are virtually stopped. It appears that KF cannot freely re-engage incomplete products and fully extend the template, even if at a very slow rate. We speculate that KF is gradually tied-up in hard-to-resolve complexes, which are mostly the result of stable secondary structure of the template or presence of an oxidative lesion. It is possible that KF continuously dissociates from a stalled reaction and re-engages the template hybridized with a partially extended primer, but simply cannot progress due to a stable secondary structure downstream.

While KF appears to be able to replicate 8-oxoG in G4 structures, we did not assess possible mutagenic effects of 8-oxoG. KF can replicate 8-oxoG with a C, which is non-mutagenic. On the other hand, a mutation can be induced by replicating 8-oxoG with A, especially if 8-oxoG is in its preferred *syn* conformation. On the template strand, this leads to a G to T transversion in subsequent replication cycles (32). The frequency of incorporation of C or A can vary significantly depending on experimental conditions (e.g. dNTP concentration), but even high-fidelity replicative polymerases bypass 8-oxoG in an error-prone manner (33–35). Whether the primers, opposed to 8-oxoG, were extended with C or A is irrelevant to our assessment of structure related polymerase stalling. Nevertheless, the frequency of misincorporation of A was probably high in our experimental setup, due to the use of KF exo$^-$, which lacks any proofreading activity.

To summarize, G-rich regions are problematic substrates for DNA polymerases and primer extension reactions can be a useful tool for probing for stable DNA secondary structure elements. Two G4 model systems, BCL2 and HTEL, effectively stall KF bypass. Our results show that the rate-limiting step is the first 3′ G involved in a regular G-quartet. On the other hand, non-G-quartet base pairs or stacked capping structures are easily bypassed by KF. Stalling upstream of second and third G-tracts suggests that triplex and hairpin unfolding intermediates are relatively stable. Oxidative lesions in the form of 8-oxoG can significantly affect the processivity of an enzyme. G4-forming sequences with more levels of redundancy in the form of additional G-tracts and long G-tracts are probably more resilient to an oxidation-induced loss of G4 structure. In systems without redundancy, 8-oxoG is most disruptive when it is located closer to the 5′-end of the G4-forming sequence, which is due to the persistence of the lesion in unfolding intermediates. Oxidative lesions likely modulate enzyme processivity and cause changes in protein expression levels.

Data availability

The data underlying this article are available in the article and in its online supplementary material.

Supplementary data

Supplementary Data are available at NAR Online.

Funding

Slovenian Research and Innovation Agency [P1-0242]. Funding for open access charge: Slovenian Research and Innovation Agency.

Conflict of interest statement

None declared.

References

1. Neidle,S. (2020) *Quadruplex Nucleic Acids as Targets for Medicinal Chemistry*. Academic Press, Cambridge, MA.
2. Sengupta,P., Bose,D. and Chatterjee,S. (2021) The molecular tête-à-tête between G-quadruplexes and the i-motif in the human genome. *Chembiochem.*, **22**, 1517–1537.
3. Estep,K.N., Butler,T.J., Ding,J. and Brosh,R.M. (2019) G4-interacting DNA helicases and polymerases: potential therapeutic targets. *Curr. Med. Chem.*, **26**, 2881–2897.
4. Valton,A.-L. and Prioleau,M.-N. (2016) G-quadruplexes in DNA replication: a problem or a necessity? *Trends Genet.*, **32**, 697–706.
5. Sato,K., Martin-Pintado,N., Post,H., Altelaar,M. and Knipscheer,P. (2021) Multistep mechanism of G-quadruplex resolution during DNA replication. *Sci. Adv.*, **7**, eabf8653.
6. Mendoza,O., Bourdoncle,A., Boulé,J.-B., Brosh,R.M. and Mergny,J.-L. (2016) G-quadruplexes and helicases. *Nucleic Acids Res.*, **44**, 1989–2006.
7. Čeru,S., Šket,P., Prislan,I., Lah,J. and Plavec,J. (2014) A new pathway of DNA G-quadruplex formation. *Angew. Chem. - Int. Ed.*, **126**, 4981–4984.
8. Grün,J.T. and Schwalbe,H. (2022) Folding dynamics of polymorphic G-quadruplex structures. *Biopolymers*, **113**, e23477.

9. Bončina,M., Lah,J., Prislan,I. and Vesnaver,G. (2012) Energetic basis of human telomeric dNA folding into G-quadruplex structures. *J. Am. Chem. Soc.*, **134**, 9657–9663.
10. Gray,R.D., Trent,J.O. and Chaires,J.B. (2014) Folding and unfolding pathways of the human telomeric G-quadruplex. *J. Mol. Biol.*, **426**, 1629–1650.
11. Takahashi,S., Brazier,J.A. and Sugimoto,N. (2017) Topological impact of noncanonical DNA structures on Klenow fragment of DNA polymerase. *Proc. Natl Acad. Sci. U.S.A.*, **114**, 9605–9610.
12. Han,H., Hurley,L.H. and Salazar,M. (1999) A DNA polymerase stop assay for G-quadruplex-interactive compounds. *Nucleic Acids Res.*, **27**, 537–542.
13. Chashchina,G.V., Tevonyan,L.L., Beniaminov,A.D. and Kaluzhny,D.N. (2023) Taq-polymerase stop assay to determine target selectivity of G4 ligands in native promoter sequences of MYC, TERT, and KIT oncogenes. *Pharmaceuticals*, **16**, 544.
14. Ren,L., Zhang,A., Huang,J., Wang,P., Weng,X., Zhang,L., Liang,F., Tan,Z. and Zhou,X. (2007) Quaternary ammonium zinc phthalocyanine: inhibiting telomerase by stabilizing G quadruplexes and inducing G-quadruplex structure transition and formation. *Chembiochem*, **8**, 775–780.
15. Palumbo,S.L., Ebbinghaus,S.W. and Hurley,L.H. (2009) Formation of a unique end-to-end stacked pair of G-quadruplexes in the hTERT core promoter with implications for inhibition of telomerase by G-quadruplex-interactive ligands. *J. Am. Chem. Soc.*, **131**, 10878–10891.
16. Kerwin,S.M., Sun,D., Kern,J.T., Rangan,A. and Thomas,P.W. (2001) G-quadruplex DNA binding by a series of carbocyanine dyes. *Bioorg. Med. Chem. Lett.*, **11**, 2411–2414.
17. Teng,F., Hou,X., Fan,S., Rety,S., Dou,S. and Xi,X. (2017) *Escherichia coli* DNA polymerase I can disrupt G-quadruplex structures during DNA replication. *FEBS J.*, **284**, 4051–4065.
18. Takahashi,S., Kim,K.T., Podbevšek,P., Plavec,J., Kim,B.H. and Sugimoto,N. (2018) Recovery of the formation and function of oxidized G-quadruplexes by a Pyrene-modified guanine tract. *J. Am. Chem. Soc.*, **140**, 5774–5783.
19. Takahashi,S., Chelobanov,B., Kim,K., Kim,B., Stetsenko,D. and Sugimoto,N. (2018) Design and properties of Ligand-conjugated guanine oligonucleotides for recovery of mutated G-quadruplexes. *Molecules*, **23**, 3228.
20. Neeley,W.L. and Essigmann,J.M. (2006) Mechanisms of formation, genotoxicity, and mutation of guanine oxidation products. *Chem. Res. Toxicol.*, **19**, 491–505.
21. Markkanen,E. (2017) Not breathing is not an option: how to deal with oxidative DNA damage. *DNA Repair (Amst.)*, **59**, 82–105.
22. Bielskutė,S., Plavec,J. and Podbevšek,P. (2019) Impact of oxidative lesions on the human telomeric G-quadruplex. *J. Am. Chem. Soc.*, **141**, 2594–2603.
23. Bielskutė,S., Plavec,J. and Podbevšek,P. (2021) Oxidative lesions modulate G-quadruplex stability and structure in the human BCL2 promoter. *Nucleic Acids Res.*, **49**, 2346–2356.
24. Luu,K.N., Phan,A.T., Kuryavyi,V., Lacroix,L. and Patel,D.J. (2006) Structure of the human telomere in K+ solution: an intramolecular (3 + 1) G-quadruplex scaffold. *J. Am. Chem. Soc.*, **128**, 9963–9970.
25. Shi,J., Wen,A., Jin,S., Gao,B., Huang,Y. and Feng,Y. (2021) Transcription activation by a sliding clamp. *Nat. Commun.*, **12**, 1131.
26. Robinson,J., Raguseo,F., Nuccio,S.P., Liano,D. and Di Antonio,M. (2021) DNA G-quadruplex structures: more than simple roadblocks to transcription? *Nucleic Acids Res.*, **49**, 8419–8431.
27. Han,X., Xu,S., Wang,L., Bi,Z., Wang,D., Bu,H., Da,J., Liu,Y. and Tan,W. (2024) Artificial DNA framework channel modulates antiapoptotic behavior in ischemia-stressed cells via destabilizing promoter G-quadruplex. *ACS Nano*, **18**, 6147–6161.
28. Turner,R.M., Grindley,N.D.F. and Joyce,C.M. (2003) Interaction of DNA polymerase I (Klenow fragment) with the single-stranded template beyond the site of synthesis. *Biochemistry*, **42**, 2373–2385.
29. Stadlbauer,P., Krepl,M., Cheatham,T.E., Koca,J. and Sponer,J. (2013) Structural dynamics of possible late-stage intermediates in folding of quadruplex DNA studied by molecular simulations. *Nucleic Acids Res.*, **41**, 7128–7143.
30. Mashimo,T., Yagi,H., Sannohe,Y., Rajendran,A. and Sugiyama,H. (2010) Folding pathways of human telomeric type-1 and type-2 G-quadruplex structures. *J. Am. Chem. Soc.*, **132**, 14910–14918.
31. Fleming,A.M., Omaga,C.A. and Burrows,C.J. (2023) NEIL3 promoter G-quadruplex with oxidatively modified bases shows magnesium-dependent folding that stalls polymerase bypass. *Biochimie*, **214**, 156–166.
32. Hahm,J.Y., Park,J., Jang,E.-S. and Chi,S.W. (2022) 8-Oxoguanine: from oxidative damage to epigenetic and epitranscriptional modification. *Exp. Mol. Med.*, **54**, 1626–1642.
33. Shibutani,S., Takeshita,M. and Grollman,A.P. (1991) Insertion of specific bases during DNA synthesis past the oxidation-damaged base 8-oxodG. *Nature*, **349**, 431–434.
34. Einolf,H.J. and Guengerich,F.P. (2001) Fidelity of nucleotide insertion at 8-oxo-7,8-dihydroguanine by mammalian DNA polymerase δ. *J. Biol. Chem.*, **276**, 3764–3771.
35. Markkanen,E., Castrec,B., Villani,G. and Hübscher,U. (2012) A switch between DNA polymerases δ and λ promotes error-free bypass of 8-oxo-G lesions. *Proc. Natl Acad. Sci. U.S.A.*, **109**, 20401–20406.

Received: June 7, 2024. **Revised:** October 11, 2024. **Editorial Decision:** October 31, 2024. **Accepted:** November 6, 2024